PCCP

Accepted Manuscript

ROYAL SOCIETY OF CHEMISTRY

www.rsc.org/pccp

PCCP

PAPER

Visible–light–driven Ag/AgCl plasmonic photocatalysts *via* a surfactant–assisted protocol: enhanced catalytic performance by morphology evolution from near–spherical to 1D structures

Received 00th January 20xx,
Accepted 00th January 20xx

DOI: 10.1039/x0xx00000x

www.rsc.org/

Yanping Wang,[ab] Penglei Chen,*[ab] Yunfan Shen,[a] Chuncheng Chen,[a] Changchun Yang[b] and Minghua Liu[a]

Ag/AgCl–based plasmonic photocatalysts have received much attention as emerging visible–light–driven photocatalysts, where those characterized with a 1D morphology have aroused great expectations. Most of the current existing protocols for the fabrication of the 1D materials, however, suffer from either multistep tedious synthesis works or the requirement of rigorous experimental conditions. A one–pot fabrication method feasible under ambient conditions is strongly desired. By means of a surfactant–assisted protocol, we report herein that Ag/AgCl structures of a near–spherical and 1D morphology could be controllably produced. We show that near–spherical Ag/AgCl species could be produced immediately after dropping an $AgNO_3$ aqueous solution into an aqueous solution of cetyltrimethylammonium chloride (CTAC) surfactant under stirring. Interestingly, we show that these initially formed near–spherical species could automatically evolve into 1D Ag/AgCl fibers simply by extending the stirring time under ambient conditions. In our new protocol, CTAC works not only as chlorine source but also as a directing reagent to assist the formation of the 1D Ag/AgCl structures. Moreover, we demonstrate that compared to the near–spherical structures, our Ag/AgCl fibers could display boosted catalytic performances towards the photodegradation of methyl orange pollutant under visible light irradiation. Our work might launch an easy method for the construction of fibrous Ag/AgCl architectures of superior photocatalytic reactivity, and it also provides deep insights into the surfactant-assisted synthesis.

1 Introduction

Over the past several decades, micro/nanostructures of a one–dimensional (1D) morphology have been catching considerable attention both from scientific and technological communities.[1–8] This is owing to their high aspect ratio and their confined dimension in the radial direction, which pave an efficient avenue for the transport of quantum particles, such as electrons, excitons, photons *etc.*, in the axial direction.[8] These issues provide 1D micro/nanostructures with versatile physicochemical properties, and thus render them fundamental curiosity and practical significance for the development of emerging advanced materials of general concern, including energy harvesting/storage/conversion systems, sensors, electronics, and others more.[1–8]

With respect to these scenarios, the development of qualified photocatalysts towards the photodegradation of organic pollutants has been recognized to be a subject of paramount importance.[8–10] This stems from the fact that with the expeditious growth of globalization and industrialization, environmental problems caused by organic pollutants have become one of the most overwhelming issues that limit the sustainable development of our society.[11–15] Numerous excellent photocatalysts, typically represented by TiO_2–based materials, have been developed to realize a photocatalytic elimination of organic pollutants.[8–15] Nevertheless, as a result of their large band gap of *ca.* 3.2 eV, UV light, which accounts for *ca.* 5% of the solar energy, is generally required for the performance of these traditional catalysts.[11–15] Considering energy utilization and saving, highly efficient photocatalysts capable of working under visible light (which accounts for *ca.* 45% of solar energy) irradiation are strongly desired.[8–15] Tremendous efforts have thus far been undertaken to initiate visible–light–energized photocatalysts, where the use of metallic nanostructures characterized with visible–light surface plasmon resonance (SPR) absorptions has been considered to be a prospective alternative towards an efficient light–to–chemical energy conversion for catalytic uses,[16–34] especially for the photodegradation of organic pollutants.[24–41] In this regard, silver/silver halides–based species have recently drawn intensive attention as promising plasmonic photocatalysts.[27–33, 35–44] This is owing to their exceptional visible–light–responsive photocatalytic performances, although silver halides conventionally function as

[a] *Beijing National Laboratory for Molecular Science, Institute of Chemistry, Chinese Academy of Sciences, No. 2 Zhongguancun Beiyijie, Beijing 100190, People's Republic of China. E–mail: chenpl@iccas.ac.cn*
[b] *College of Chemistry and Molecular Engineering, Zhengzhou University, 100 Science Road, Henan, Zhengzhou 450001, People's Republic of China. E–mail: cpl@zzu.edu.cn*

† Electronic Supplementary Information (ESI) available: The EDX elemental analysis of our Ag/AgCl nanostructures. The SEM images of our Ag/AgCl nanostructures produced by various controlled experiments, and the real–time absorption spectra of MO molecules during the photodegradation process. See DOI: 10.1039/x0xx00000x

the primary source material in photographic plates and are unstable upon photoirradiation.[27–33, 35–41]

While the past a few years have witnessed rapid advancements in terms of silver/silver halides-based plasmonic photocatalysts of a spherical, cubic, concave cubic, sheetlike, dendritic and polyhedra morphology,[25–33, 35–41] those of a 1D architecture have also received great interest and become a hot topic of this direction.[45–54] Currently, a couple of 1D silver/silver halide species of excellent photocatalytic performances have been fabricated.[45–54] In some cases, the fabrication, however, suffers from either multistep and laborious synthesis works or the requirement of high pressure and high temperature.[45–47] In some other cases, either metallic Ag species of a 1D morphology, which are prefabricated by a complicated process,[48–52] or metallic Ag foils,[54] are transformed to 1D silver/silver halides structures *via* a partial oxidation–halidation process.[48–54] This makes the fabrication a tedious work. Accordingly, despite the great successes in fabricating 1D silver/silver halide structures,[45–54] the initiation of an one–pot protocol, which is feasible under ambient conditions using silver salt as Ag source, still remains a formidable challenge.

To address this significant issue, we herein report our new findings that by means of a one–step reaction between $AgNO_3$ and cetyltrimethylammonium chloride (CTAC) surfactant under ambient conditions, near–spherical and 1D Ag/AgCl structures could be controllably produced simply by tuning the reaction time. It is found that when an $AgNO_3$ aqueous solution is added into a CTAC aqueous solution under stirring, near–spherical Ag/AgCl species could be produced immediately after the adding of $AgNO_3$. Fascinatingly, these near–spherical Ag/AgCl structures could automatically evolve into 1D species simply by extending the stirring time. Moreover, we show that compared to the near–spherical Ag/AgCl structures, the 1D counterparts exhibit distinctly boosted catalytic reactivity towards photodegradation of methyl orange (MO) pollutants under visible–light irradiation. So far as we know, this might be the first report that 1D Ag/AgCl structures could be produced under ambient conditions *via* a one–pot method directly by using silver salt as Ag source. On one hand, our investigation might pave a new and facile avenue for one–pot fabrication of 1D plasmonic Ag/AgCl structures of superior visible–light–driven photocatalytic performances. On the other hand, in terms of a morphology evolution, it sheds deep scientific insights into the surfactant–assisted synthesis, which is among the most important fabrication protocols.[54– 56]

2 Experimental section

2.1 Chemicals and reagents

Cetyltrimethylammonium chloride (CTAC, Alfa Aesar, 96%), silver nitrate ($AgNO_3$, Alfa Aesar, >99%), and methyl orange (MO, Alfa Aesar, >98%), were used as received without further purification or treatment. Milli–Q water (18 MΩ cm) was used as solvent in all cases.

2.2 One–pot synthesis of Ag/AgCl architectures *via* a surfactant–assisted protocol

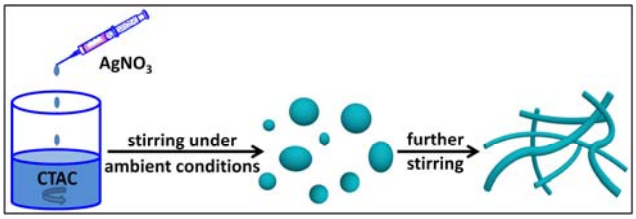

Scheme 1 A schematic illustration for the fabrication of 1D Ag/AgCl structures *via* a one–pot surfactant–assisted protocol, wherein fibrous architectures could be produced simply by a longer stirring time under ambient conditions.

To fabricate the near–spherical Ag/AgCl structures, an aqueous solution of $AgNO_3$ (600 μL, 5×10^{-2} mol L^{-1}) was dropwise added into an aqueous dispersion of CTAC surfactant (10 mL, 4×10^{-2} mol L^{-1}) under vigorous magnetic stirring and under ambient conditions without special protection. The volume of the vial employed for the synthesis was *ca.* 25 mL. The speed of the magnetic stirring was around 1500 rpm. The ambient temperature was in the range of 16~30 ^{o}C. In this protocol, CTAC surfactant functioned as chlorine source and also as the directing reagent for the formation of the near–spherical structures, while $AgNO_3$ worked as the silver source. After the stirring was maintained under ambient conditions for 20 minutes, the as–obtained dispersion was treated by centrifugation (10000 rpm, 5 minutes), and the produced solids were collected and washed thoroughly with ultrapure Milli–Q water by repeating centrifugations (10000 rpm, 10 minutes). To produce 1D structures, nearly similar operations were carried out, except that a stirring time of 36 hours was applied. The as–synthesized products were then subjected to various characterizations or to photocatalytic uses.

2.3 Photocatalytic performances

To achieve the photocatalytic performances, photocatalysts typically involving *ca.* 2 mg of Ag/AgCl structures were dispersed in an aqueous solution of MO pollutant (4 mL, 20 mg L^{-1}), wherein a quartz cuvette was used as the reactor. A 500 W xenon arc lamp, which was installed in a laboratory lamp housing system (CHF–XM35–500 W, Beijing Trusttech Co. Ltd., China) was used as the light source. Before entering the reactor, the light passed through a 10 cm water filter and a UV cutoff filter (>420 nm). Practically, before the light irradiation, the reaction system was kept for 30 minutes in a dark room to achieve an equilibrium adsorption state. The dark adsorption time was appointed to be 30 minutes since we found that, when a longer adsorption time of 24 hours was applied, similar results were obtained. During the photocatalytic reactions, an aliquot of the dispersion (0.3 mL) was taken out from the reaction system for real–time sampling. The progress of the photocatalytic elimination of MO pollutants over our Ag/AgCl plasmonic photocatalysts was monitored by detecting the real–time UV–vis absorption of MO molecules at *ca.* 463 nm. For the evaluation of the photocatalytic reactivity, C was the concentration of the MO molecules at a desired real–time t, and C_0 was that immediately before it was kept in the dark. The rate constant of the photocatalytic reaction, with regard to the correlation between $\ln(C/C_0)$ and the reaction time (t), was extracted by a kinetic linear simulation of the curves of the photocatalytic performances.

2.4 Fabrication of electrodes and electrochemical measurements

For the electrochemical impedance spectral (EIS) investigations, the electrode was fabricated by a modification of indium tin oxide (ITO) glass electrodes using our Ag/AgCl structures. To achieve this, *ca.* 7.5 mg Ag/AgCl were dispersed in Nafion water solution, and the produced paste was spread on the surface of ITO electrode (2 cm × 2 cm) and dried under ambient conditions. The electrochemical impedance measurements were performed on a conventional three–electrode cell using a CHI 660B potentiostat/galvanostat (Shanghai Chenhua Instrumental Co., Ltd., China) at room temperature. Herein, a platinum wire worked as the counter electrode and a saturated calomel (saturated KCl) electrode (SCE) worked as the reference electrode, while the modified ITO electrode served as the working electrode. The measurement was carried out in the presence of 2.5 mM $K_3[Fe(CN)_6/K_4[Fe(CN)_6]$ (1:1) mixture as a redox probe in 0.1 M KCl solution. The impedance spectra were recorded with the help of ZPlot/ZView software under an ac perturbation signal of 5 mV over the frequency range from 10 k Hz to 0.1 Hz at a potential of 0.1 V. The photocurrent experiments were also performed in the three−electrode system. Here, the working electrode was intermittently irradiated with visible−light during the measurements, and the photocurrent−time characteristics were recorded with the electrochemical analyzer.

2.5 Apparatus and measurements

The scanning electron microscopy (SEM) investigations were carried out using a Hitachi S−4800 system. The energy dispersive X−ray spectroscopy (EDX) was detected with a Horiba EMAX X−act energy dispersive spectroscopy that was attached to the Hitachi S−4800 system. The UV−vis diffuse reflectance spectra of the samples were obtained on an UV−vis spectrophotometer (Hitachi U−3010) using $BaSO_4$ as the reference. The X–ray photoelectron spectroscopy (XPS) was performed on an ESCALab220i–XL electron spectrometer from VG Scientific using 300 W Al Kα radiation. The powder X–ray diffraction (PXRD) measurements were performed on a PANalytical X'Pert PRO instrument with Cu Kα radiation. The photocatalytic degradation of the MO pollutants was monitored by measuring the real−time UV−vis spectra of the catalytic systems using a Hitachi U−3010 spectrometer. All the measurements were carried out under ambient conditions.

3 Results and discussion

3.1 Near–spherical and 1D Ag/AgCl structures *via* a surfactant–assisted protocol

Practically, as schematically illustrated in Scheme 1, our Ag/AgCl structures were synthesized *via* a simple surfactant–assisted fabrication protocol under ambient conditions. The obtained products were examined by SEM. As shown in Fig. 1A and 1B, near–spherical structures of *ca.* 120~700 nm were produced when the synthesis dispersion was stirred under ambient conditions for 20 minutes. Interestingly, it was found that most of these near–spherical species formed at the initial stage evolved into 1D architectures of a diameter of *ca.* 150~500 nm and a length of *ca.* 2~10 μm when the stirring time was further extended to 36 hours, as shown in Fig. 1C and 1D.

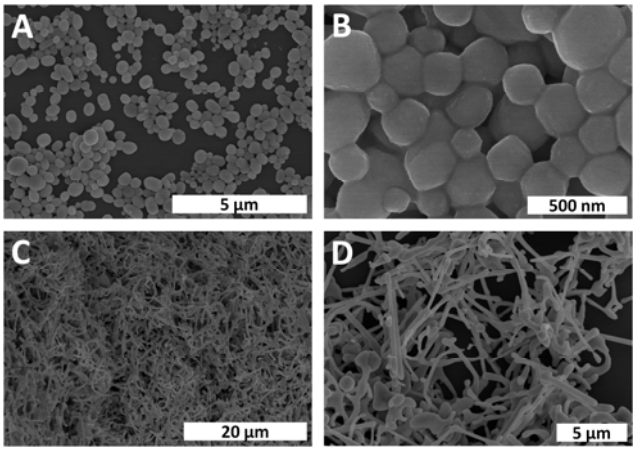

Fig. 1 The typical SEM images of the as–produced near–spherical (A and B) and fibrous (C and D) Ag/AgCl structures.

The component of the as–manufactured products was investigated by means of EDX analysis. As shown in Fig. S1, EDX signals ascribing to silicon element could be detected from our samples, since silicon slices were employed as the solid support for the measurements. In the case of the near–spherical structures, silver and chlorine elements could be distinctly detected. A semiquantitative analysis indicates that the atomic ratio between Ag and Cl elements is about 1.02:1. This value is higher than the theoretic stoichiometric atomic ratio between Ag and Cl species of AgCl, which should be 1:1. This result preliminarily implies an ambient light induced generation of metallic Ag^0 species in the near–spherical structures, which leads to the formation of Ag/AgCl composites.[32, 33, 37, 40, 41] This could be experimentally verified by means of XPS investigations. As shown in Fig. 2A, the Cl species exhibit a binding energy of Cl $2p_{3/2}$ and Cl $2p_{1/2}$ around 197.7 and 199.3 eV, respectively.[57] In addition, as presented in Fig. 2B, two bands at *ca.* 367.3 and 373.4 eV, which could be attributed to Ag $3d_{5/2}$ and Ag $3d_{3/2}$ binding energies, respectively, could also be detected. In terms of a deconvolution treatment, these two bands could be further deconvoluted into two sets of peaks at 367.3, 368.4 eV, and 373.4, 374.4 eV, respectively. Those at 367.3 and 373.4 eV could be ascribed to the Ag^+ species of AgCl, while those at 368.4 and 374.4 eV could be attributed to the metallic Ag^0 species.[28, 32, 40] The semiquantitatively calculated mole ratio between Ag^0 and Ag^+ is approximately 1:35. These experimental facts affirm the existence of Ag^0 species in the as–produced near–spherical structures, further suggesting the ambient light induced generation of Ag^0 species, which results in the production of Ag/AgCl species.[32, 33, 37, 40, 41] As shown in Fig. S1B, 2C and 2D, appromximately similar EDX and XPS results are obtained in the case of the 1D structures, implying that our spheres and 1D fibers basically have similar component.

For visible–light–driven photocatalysts, it is substantially required that the catalysts could exhibit evident absorptions in the visible region.[12, 13] The UV–visible diffuse reflectance spectra of our near–spherical and fibrous structures were investigated. As shown in Fig. 3, besides the absorptions in the ultraviolet region, which are attributed to AgCl species, broad and strong absorptions in the

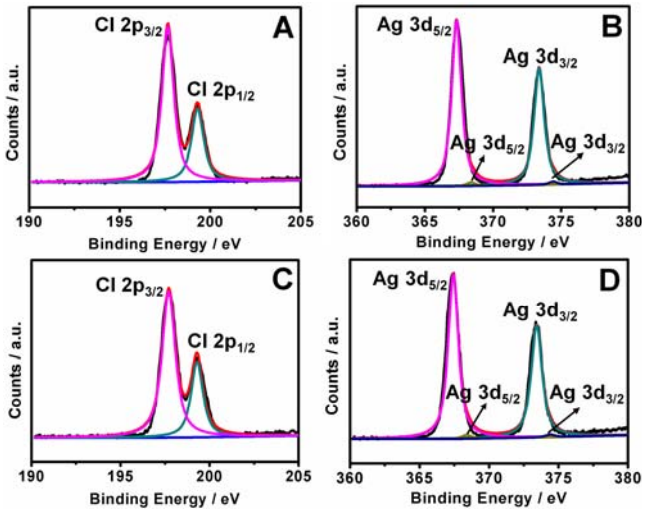

Fig. 2 The typical XPS spectra of Cl 2p (A and C) and Ag 3d (B and D) of our near–spherical (A and B) and fibrous (C and D) structures.

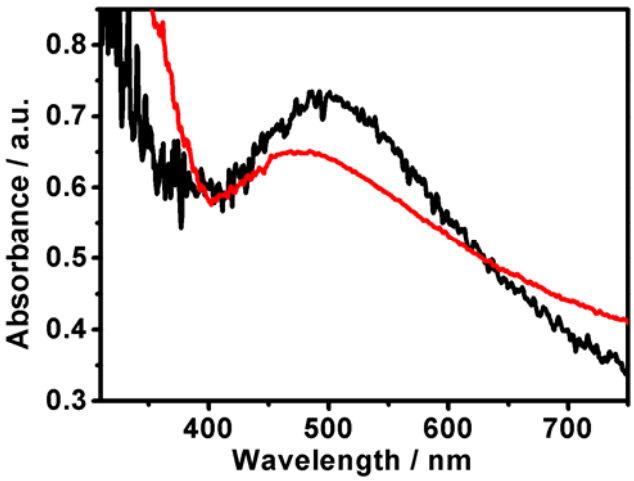

Fig. 3 The UV–visible diffuse reflectance spectra of our near–spherical (black) and fibrous (red) structures.

visible region could also be distinctly detected from both of the structures. Generally, bare AgCl materials could only display evident absorptions in the ultraviolet region but nearly negligible absorptions in the visible region.[28] Accompanied by the experimental facts of EDX and XPS shown in Fig. S1 and Fig. 2, respectively, these present results further indicate the ambient light–induced generation of metallic Ag^0 species in our products,[32, 33, 37, 40, 41] which can arouse SPR absorptions in the visible region.

The morphology evolution process from the near–spherical to the fibrous structures was investigated by means of measuring the SEM images of the products formed at different aging times. As shown in Fig. S2A, it can be seen that, when the stirring time was 1 hour, besides spherical structures, a couple of 1D structures with a diameter of *ca.* 150~500 nm and a length of *ca.* 0.6~2 μm could also be observed. On the other hand, when the aging time was further increased to 12 hours (Fig. S2B), the relative amount of the 1D structures (a diameter of *ca.* 150~500 nm and a length of *ca.* 0.6~10 μm) increased with a decreased amount of the spherical structures. Moreover, the relative amount of the 1D structures (a diameter of *ca.* 150~500 nm and a length of *ca.* 2~10 μm) were further increased when the stirring time was increased to 24 hours (Fig. S2C). When an even longer aging time of 48 and 72 hours was employed (Fig. S2D, and S2E), fibrous structures, which are similar to those obtained with an aging time of 36 hours (Fig. 1B and 1C), are observed. It should be noted that *ca.* 2 mg spherical structures could be obtained when the synthesis system was stirring for 20 minutes. This value was almost similar to that of the 1D structures, which were produced by using an aging time of 36, 48 or 72 hours. These experimental results indicated that the formation of our 1D structures might be, to a great extent, achieved *via* a morphology transformation/evolution but not *via* a further growth of the spherical structures.[58–60]

To study how the near–spherical structures were transformed into 1D fibers, a controlled experiment was performed, wherein the near–spherical Ag/AgCl structures, which were produced by stirring the reaction system for 20 minutes and were washed thoroughly with pure Mill–Q water, were redispersed into plain water, in which no CTAC surfactants were contained. The as–obtained dispersion was stirred under ambient conditions for 36 hours, after which the products were collected *via* centrifugation and were subjected to SEM investigation. As shown in Fig. S3, such pure water–treated samples manifest themselves also as near–spherical structures. Together with the above–mentioned fact that the 1D Ag/AgCl fibers were produced when the original reaction system was stirred for 36 hours in the presence of CTAC (4×10^{-2} mol L^{-1}), these experimental facts indicated that the CTAC surfactant might play an important role for the morphology evolution from the near–spherical to the fibrous architectures.

To confirm this, we carried out a couple of other controlled experiments, wherein the near–spherical Ag/AgCl precursors, which had been washed with Mill–Q water, were re–dispersed in a CTAC aqueous solution of a low–concentration (4×10^{-3} mol L^{-1}) and a high–concentration (4×10^{-2} mol L^{-1}). The as–obtained dispersions were stirred under ambient conditions for 36 hours, and the SEM images of the products were measured after being washed with water adequately. As shown in Fig. S4, in the case of the samples treated by a CTAC aqueous solution of a low–concentration, near–spherical Ag/AgCl structures are observed from the SEM images. In contrast, it is interesting to find that 1D fibers could be observed for the samples that treated with a CTAC aqueous solution of a high–concentration, as shown in Fig. S5.

As it is widely known, CTAC surfactant is one of the most frequently addressed directing reagents for controllable synthesis, and the shape of the produced structures could be directed by the shape of the micelles,[57, 61–67] wherein surfactant concentration is one of the most important issues that could affect the shape of the micelles.[68, 69] Generally, for surfactant–assisted controllable fabrication, isotropically–shaped spherical structures are inclined to be produced when a surfactant solution of a low–concentration is used. This is directed by the spherical micelles formed at low–concentration. In contrast, anisotropically–shaped 1D structures are inclined to be produced when a surfactant solution of a high–concentration is used. This is directed by the 1D wormlike micelles formed at high–concentration.[56, 65, 68, 70] On the basis of the

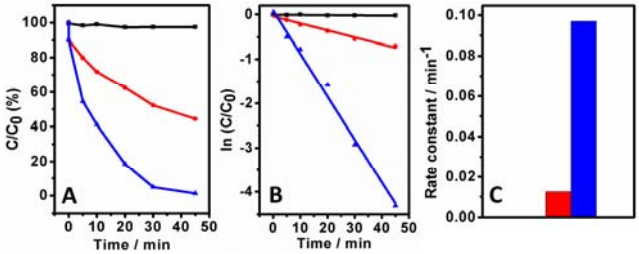

Fig. 4 Photocatalytic performances (A) and the corresponding kinetic linear simulation curves (B) of our photocatalysts (black curve: a blank experiment, wherein no catalyst is used; red curve: near–spherical Ag/AgCl structures are used as the photocatalysts; blue curve: fibrous Ag/AgCl structures are used as the photocatalysts) towards the photodegradation of MO pollutants. Panel C: a histogram of the reaction rate constants over our near–spherical (red) and fibrous (blue) Ag/AgCl structures.

aforementioned experimental facts and together with these concise backgrounds, a plausible scenario could be tentatively proposed for our interesting morphology evolution phenomenon. When a guest solution containing $AgNO_3$ was dropped into a host solution containing CTAC surfactants, near–spherical Ag/AgCl species were formed at the initial stage of the reaction, owing to the well–known poor solubility of AgCl in aqueous systems. Here, ambient light induced the generation of Ag^0 species,[32, 33, 37, 40, 41] while the CTAC surfactant worked as the directing reagent to assist the formation of the near–spherical structures.[55, 56, 58, 68, 69] Nevertheless, during the further aging of the dispersions, the ionization of the as–formed near–spherical structures would release Ag^+ species. When plain water or a low–concentration CTAC aqueous solution is employed as the aging medium, a balanced state would be eventually reached, and the near–spherical structures would maintain their morphology (Fig. S3, and S4). This is owing the lack of 1D wormlike micelles, which are basically favored by a high–concentration surfactant solution.[56, 65, 68, 70] In contrast, when a high–concentration CTAC aqueous solution is used as the aging medium, the released Ag^+ species would react with Cl^-, wherein the resulted products were induced to form 1D structures (Fig. 1C, 1D and S5). In this case, the 1D wormlike micelles favored by the high–concentration surfactants worked as the soft templates to induce the formation of the 1D structures.[56, 65, 68, 70]

This could be further confirmed by means of another controlled experiment, wherein an aqueous solution of $AgNO_3$ was dropwise added into a low–concentration CTAC aqueous solution (4×10^{-3} mol L^{-1}) under stirring. In this case, it was demonstrated that near–spherical structures could also be produced at the initial stage of the reaction. The as–manufactured products, however, maintained their near–spherical morphology unchanged even after the reaction dispersion was stirred for 36 hours, as shown in Fig. S6. Accompanied by the information deduced from the other controlled experiments, and accompanied by the above-mentioned brief backgrounds,[56, 65, 68, 70] these results further confirm that the directing effects of the 1D wormlike micelles favored by high–concentration CTAC surfactants might play a crucial role for the near–spherical to fibrous morphology evolution.

3.2 Morphology–dependent photocatalytic performances of the near–spherical and fibrous Ag/AgCl structures

On one hand, it can be seen from the above sections that our Ag/AgCl structures could display broad and intense SPR absorptions in the visible region (Fig. 3). This might endow them with photocatalytic reactivity under visible light irradiations.[12, 13] On the other hand, the successful fabrication of the near–spherical and 1D structures provides us with good opportunities to investigate their morphology–dependent photocatalytic performances. As shown in Fig. 4A and S7A, when no catalysts are used in the photoreaction system, only negligible photodegradation of MO molecules could be observed under visible–light irradiation. This result indicates that the self–photo–sensitized degradation of MO molecules under our experimental conditions could be substantially ignored.

In contrast, when our near–spherical Ag/AgCl structures are involved in the reaction system, *ca.* 44% MO molecules are decomposed within 45 minutes, as shown in Fig. 4A and Fig. S7B. This indicates that our near–spherical Ag/AgCl could work as visible–light–driven plasmonic photocatalysts towards the photodegradation of MO. In contrast, when our Ag/AgCl fibers are used, nearly 100% MO molecules are decomposed under the similar conditions. As plotted in Fig. 4B, a good linear correlation between $\ln(C/C_0)$ and t could be observed. This indicates that the decomposition reaction of MO over our Ag/AgCl plasmonic photocatalysts follows the first–order kinetics, $-dC/dt = kC$, wherein k is the rate constant of the reaction. As shown in Fig. 4B, it can be seen that the rate constant of the MO degradation reaction over our 1D Ag/AgCl fibers are determined to be 9.7×10^{-2} min^{-1}. This value is nearly 6.1 times higher than that of 1.6×10^{-2} min^{-1} over our near–spherical structures. These results indicate that compared to the near–spherical counterparts, our 1D Ag/AgCl architectures are superior visible–light–driven plasmonic photocatalysts of substantially boosted catalytic reactivity. This could be clearly seen from the histogram of the rate constants shown in Fig. 4C.

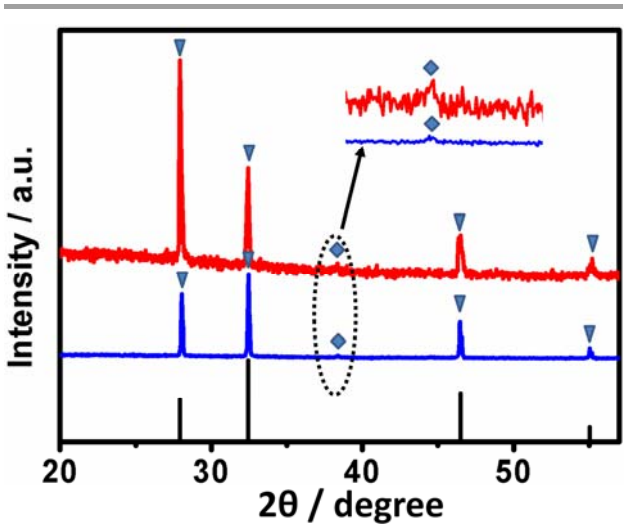

Fig. 5 The PXRD patterns of the standard JCPDS file of AgCl (black) and of our near–spherical (blue curve) and fibrous (red curve) Ag/AgCl structures. The diffraction peaks ascribed to the AgCl and Ag^0 species are marked with ▼ and ◆, respectively.

Generally, it is known that an efficient charge separation/transfer is one of the most critical issues that could affect the photocatalytic reactivity of a photocatalyst.[13, 71] It has been demonstrated that the so–called morphology–dependent catalytic reactivity could generally be understood with regard to the different catalytic reactivity induced by specific crystal facets enriched in an anisotropically shaped architecture.[72–74] Thus far, numerous qualified catalysts have been identified in terms of morphology–sensitive catalytic behaviors.[72–74] To elucidate this issue in our present case, the PXRD patterns of our structures were examined. As shown Fig. 5, distinct diffraction peaks located at *ca.* 55.0°, 46.3°, 32.3° and 27.9°, which could be indexed to the {311}, {220}, {200}, and {111} facets of the typical cubic phase AgCl (JCPDS file: 31–1238), respectively, could be observed from their PXRD.[28] Meanwhile, a weak diffraction peak at *ca.* 38.2°, which could be attributed to the {111} facet of the cubic phase metallic Ag (JCPDS file: 65–2871), could also be observed.[40] Accompanied by the experimental facts of EDX (Fig. S1) and XPS (Fig. 2), and the SPR absorptions observed in the visible region (Fig. 3), these reuslts further confirm the formation of Ag/AgCl composites.

It is interesting to note that in the PXRD pattern of our 1D architectures (Fig. 5, red curve), the intensity ratio of the AgCl {111} peak to that of {200} peak, estimated using {200} as a reference, is *ca.* 2.2. This value is substantially higher than that of the standard JCPDS file of AgCl, which is generally *ca.* 0.5. The observation of the extraordinary protuberant {111} peak implies that the AgCl of our fibrous Ag/AgCl might be enriched with {111} facets relatively. In contrast, as shown in Fig. 5 (blue curve), in the case of the PXRD curve of our near–spherical structures, almost a similar pattern as that of the fibers is observed, except that the intensity ratio of the AgCl {111} peak to that of {200} peak, is *ca.* 0.7. This value is smaller than that of our 1D Ag/AgCl and is close to that of the standard JCPDS file of AgCl, indicating that the the AgCl of our near–spherical Ag/AgCl might mainly be enriched with mixed crystal planes, wherein the relative content of the AgCl {111} and AgCl {100} facets is lower and higher than those of our 1D Ag/AgCl, respectively. Experimentally, we have also attempted to disclose the structure of our Ag/AgCl by means of TEM. However, during the measurements, we unfortunately found that these materials suffered a fast decomposition soon after the focusing. As a matter of fact, a similar phenomenon has been reported previously,[31, 40, 75] wherein it has been found that the Ag/AgCl are rapidly destroyed by the high–energy electron beam during the TEM investigation. Nevertheless, as indicated by our experimental results of PXRD (Fig. 5), compared with their spherical counterparts, the 1D structures possessed a higher content of AgCl {111} facet. In terms of PXRD, similar crystalline structure analysis has been reported for face–centered cubic phase of silver halides.[35–37]

For photocatalysts based on silve halide species, it has been demonstrated that their {111} facets could display a higher catalytic reactivity compared to the {100} facets.[35–39] As known, the AgCl {111} facets possess a layered structure, which is characterized by Ag^+ slabs interleaved with Cl^- slabs.[35–38] This would induce a static electric field perpendicular to the AgCl {111} facets, which could promote an effective photoinduced electron–hole separation, thus endowing AgCl {111} with superior catalytic reactivity.[37] In contrast, the slabs of the AgCl {100} facets are composed of both Ag^+ and Cl^- species,[35–38] which could not induce a surface perpendicular static electric field.[37] Consequently, the promoted photoinduced electron–hole separation occurring in the case of AgCl {111} facets could not ocurr in AgCl {100} facets. Thus, compared to AgCl {100} facets, the AgCl {111} facets exhibit relatively more effective photoinduced electron–hole separation capability. This endows AgCl speices of enriched {111} facts with superior catalytic reactivity comparatively.[35–39] Based on these basic understandings and accompanied by our experimental results of PXRD investigations shown in Fig. 5, we suggested that this issue might contribute, to some extent, to the higher photocatalytic performances of our 1D structures. Similar proposals have been reported for the enhanced photocatalytic performances of silver/silver halides–based photocatalysts.[35–39]

On the other hand, it is widely known that among the various sophisticated applications of 1D structures, those for catalytic uses have received particular attention.[7–10] This is owing to their intrinsic large aspect ratio and their limited dimension in the radial direction,

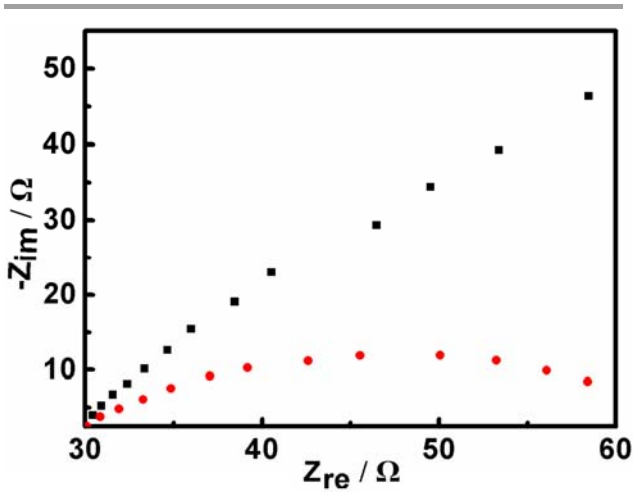

Fig. 7 The typical EIS spectra of the ITO electrodes modified by our near–spherical (black) and fibrous (red) Ag/AgCl structures.

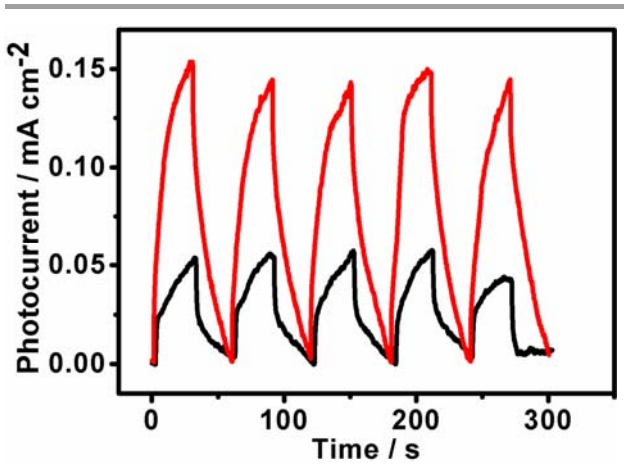

Fig. 6 The typical transient photocurrent responses of the ITO electrodes modified by our near–spherical (black curve) and fibrous (red curve) Ag/AgCl structures.

which paves a good avenue for an efficient charge transport with a reduced grain boundary. This endows them with superior charge transport capabilities, which play an important role for the enhancement of photocatalytic performances.[50, 76–81] On the basis of these issues, and together with the aftermentioned results of the transient photocurrent responses and EIS spectra of our Ag/AgCl–based materials, we tentatively suggest that the more powerful electron–hole separation and charge transport capacity of our fibers synergistically endowed by their enriched AgCl {111} facets and their 1D structural feature might contribute greatly to their distinctly boosted photocatalytic reactivity.

In order to experimentally disclose that our fibrous Ag/AgCl structures possess a more efficient electron–hole separation and charge transport capability, their transient photocurrent responses towards the intermittent visible–light irradiations were studied with regard to photocurrent–time response (*I*–*t*) curves. It can be seen from Fig. 6 that an increased photocurrent is observed when the light irradiation is switched on, while a decreased photocurrent is observed when the light irradiation is switched off. Such reversible photocurrent responses could be performed reproducibly and repeatedly over a couple light switched–on/off cycles. These results suggeste the separation and transportation of the photogenerated electron–hole pairs in our samples upon light irradiation. Specifically speaking, for the ITO electrodes modified by our near–spherical Ag/AgCl structures, relatively slight photocurrent responses with weak current intensity could be observed. Comparatively, in the case of the ITO electrodes modified by our 1D Ag/AgCl architectures, distinct photocurrent responses with an evidently boosted photocurrent intensity could be observed. These observations indicate that compared to the near–spherical structures, there exist promoted charge separation/transfer and suppressed recombination of electron–hole pairs in the 1D fibers. This is in good accordance to the photocatalytic results that compared to the near–spherical Ag/AgCl structures, our 1D species could exhibit enhanced catalytic performance (Fig. 4 and S6).

To further support our proposals, the EIS of our Ag/AgCl were investigated in terms of Nyquist plots. As illustrated in Fig. 7, the size of the arc radius of the electrodes modified by our 1D Ag/AgCl architectures is evidently smaller than that of the electrodes modified by the near–spherical species. This suggests a decrease in the solid state interface layer resistance and the charge transfer resistance on the surface of our 1D structures.[82, 83] Accompanied by the above–mentioned results of transient photocurrent responses (Fig. 6), this further confirms that compared to their counterparts of a near–spherical morphology, the more efficient photoinduced electron–hole separation/tansport ocurred in our 1D structures confer them with superior catalytic performances.

4 Conclusions

In summary, simply by means of extending the stirring time under ambient conditions, we demonstrate for the first time that Ag/AgCl plasmonic photocatalysts of a 1D morphology could be formulated by means of a one–pot surfactant–assisted protocol. In our new method, CTAC surfactant works not only as chlorine source but also serves as soft templates to assist the formation of 1D Ag/AgCl structures. Furthermore, it is found that in contrast to the near–spherical Ag/AgCl structures, which are formulated by using a short stirring time, the as–fabricated 1D Ag/AgCl architectures could display a substantially enhanced photocatalytic performance towards the photodegradation of MO molecules. With regard to a surfactant-assisted morphology evolution, our investigation might initiate a new and facile way for a one–pot synthesis of 1D Ag/AgCl of superior catalytic performances.

Acknowledgements

We acknowledge the financial support from the National Natural Science Foundation of China (Grants 21372225, 20873159, 21321063, and 91027042), the National Key Basic Research Project of China (Grants 2013CB834504 and 2011CB932300), and the Chinese Academy of Sciences (Grants XDA09030200 and 1731300500015). The authors also thank Prof. Dr. Yilin Wang, Wanhong Ma, and Dr. Xiang Hao from Institute of Chemistry, Chinese Academy of Sciences, for their helpful discussions on the surfactant–assisted synthesis, the photocatalytic performances, and the PXRD analysis, respectively.

Notes and references

1 H.–W. Liang, J.–W. Liu, H.–S. Qian and S.–H. Yu, *Acc. Chem. Res.,* 2013, **46,** 1450–1461.
2 Y. Xia, P. Yang, Y. Sun, Y. Wu, B. Mayers, B. Gates, Y. Yin, F. Kim and H. Yan, *Adv. Mater.,* 2003, **15,** 353–389.
3 J. Tian, Z. Xu, C. Shen, F. Liu, N. Xu and H.–J. Gao, *Nanoscale,* 2010, **2,** 1375–1389.
4 X. Zhao, B. Cai, Q. Tang, Y. Tong and Y. Liu, *Sensors,* 2014, **14,** 13999–14020.
5 J. L. Xie, C. X. Guo and C. M. Li, *Energy Environ. Sci.,* 2014, **7,** 2559–2579.
6 Q. H. Cui, Y. S. Zhao and J. Yao, *Chem. Sci.,* 2014, **5,** 52–57.
7 H. Sun, J. Deng, L. Qiu, X. Fang and H. Peng, *Energy Environ. Sci.,* 2015, **8,** 1139–1159.
8 B. Weng, S. Liu, Z.–R. Tang and Y.–J. Xu, *RSC Adv.,* 2014, **4,** 12685–12700.
9 J. Tian, Z. Zhao, A. Kumar, R. I. Boughton and H. Liu, *Chem. Soc. Rev.,* 2014, **43,** 6920–6937.
10 K. Lee, A. Mazare and P. Schmuki, *Chem. Rev.,* 2014, **114,** 9385−9454.
11 O. Legrini, E. Oliveros and A. M. Braun, *Chem. Rev.,* 1993, **93,** 671−698.
12 A. Kubacka, M. Fernández–García and G. Colón, *Chem. Rev.,* 2012, **112,** 1555−1614.
13 C. Chen, W. Ma and J. Zhao, *Chem. Soc. Rev.,* 2010, **39,** 4206−4219.
14 A. Mills, R. H. Davies and D. Worsley, *Chem. Soc. Rev.,* 1993, **22,** 417−425.
15 M. R. Hoffmann, S. T. Martin,W.Choi and D. W. Bahnemann, *Chem. Rev.,* 1995, **95,** 69−96.
16 H. Wang, T. You, W. Shi, J. Li and L. Guo, *J. Phys. Chem. C,* 2012, **116,** 6490−6494.
17 K. Awazu, M. Fujimaki, C. Rockstuhl, J. Tominaga, H. Murakami, Y. Ohki, N. Yoshida and T. Watanabe, *J. Am. Chem. Soc.,* 2008, **130,** 1676−1680.
18 P. Christopher, H. Xin and S. Linic, *Nat. Chem.,* 2011, **3,** 467−472.
19 Z. Liu, W. Hou, P. Pavaskar, M. Aykol and S. B. Cronin, *Nano Lett.,* 2011, **11,** 1111–1116.

20 X. Chen, H.–Y. Zhu, J.–C. Zhao, Z.–F. Zheng and X.–P. Gao, *Angew. Chem. Int. Ed.,* 2008, **47,** 5353–5356.
21 H. Zhu, X. Ke, X. Yang, S. Sarina and H. Liu, *Angew. Chem. Int. Ed.,* 2010, **49,** 9657–9661.
22 S. Linic, P. Christopher and D. B. Ingram, *Nat. Mater.,* 2011, **10,** 911–921.
23 S. Sarina, E. R. Waclawik and H. Zhu, *Green Chem.,* 2013, **15,** 1814–1833.
24 Q. Xiao, E. Jaatinen and H. Zhu, *Chem. Asian J.,* 2014, **9,** 3046–3064.
25 Z. Lou, Z. Wang, B. Huang and Y. Dai, *ChemCatChem,* 2014, **6,** 2456–2476.
26 X. Zhou, G. Liu, J. Yu and W. Fan, *J. Mater. Chem.,* 2012, **22,** 21337–21354.
27 P. Wang, B. Huang, Y. Dai and M.–H. Whangbo, *Phys. Chem. Chem. Phys.,* 2012, **14,** 9813–9825.
28 P. Wang, B. Huang, X. Qin, X. Zhang, Y. Dai, J. Wei, and M.–H. Whangbo, *Angew. Chem. Int. Ed.,* 2008, **47,** 7931–7933.
29 C. An, S. Peng and Y. Sun, *Adv. Mater.,* 2010, **22,** 2570–2574.
30 H. Xu, H. Li, J. Xia, S. Yin, Z. Luo, L. Liu and L. Xu, *ACS Appl. Mater. Interfaces,* 2011, **3,** 22–29.
31 J. Jiang and L. Zhang, *Chem. Eur. J.,* 2011, **17,** 3710–3717.
32 M. Zhu, P. Chen and M. Liu, *ACS Nano,* 2011, **5,** 4529–4536.
33 M. Zhu, P. Chen and M. Liu, *Langmuir,* 2012, **28,** 3385−3390.
34 C. Zhang, Y. Li, D. Wang, W. Zhang, Q. Wang, Y. Wang and P. Wang, *Environ. Sci. Pollut. Res.,* 2015, **22,** 10444–10451.
35 H. Wang, J. Gao, T. Guo, R. Wang, L. Guo, Y. Liu and J. Li, *Chem. Commun.,* 2012, **48**, 275–277.
36 H. Wang, J. Yang, X. Li, H. Zhang, J. Li and L. Guo, *Small,* 2012, **8,** 2802–2806.
37 Y. Shen, P. Chen, D. Xiao, C. Chen, M. Zhu, T. Li, W. Ma and M. Liu, *Langmuir,* 2015, **31,** 602−610.
38 Z. Lou, B. Huang, X. Ma, X. Zhang, X. Qin, Z. Wang, Y. Dai and Y. Liu, *Chem. Eur. J.,* 2012, **18,** 16090–16096.
39 Z. Lou, B. Huang, X. Qin, X. Zhang, H. Cheng, Y. Liu, S. Wang, J. Wang and Y. Dai, *Chem. Commun.,* 2012, **48**, 3488–3490.
40 M. Zhu, P. Chen, W. Ma, B. Lei and M. Liu, *ACS Appl. Mater. Interfaces,* 2012, **4,** 6386−6392.
41 M. Zhu, P. Chen and M. Liu, *Langmuir,* 2013, **29,** 9259−9268.
42 D. Wang, Y. Li, G. L. Puma, C. Wang, P. Wang, W. Zhang and Q. Wang, *Chem. Commun.,* 2013, **49**, 10367–10369.
43 D. Wang, Y. Li, G. L. Puma, C. Wang, P. Wang, W. Zhang and Q. Wang, *J. Hazard. Mater.,* 2015, **285,** 277–284.
44 D. Wang, Y. Li, G. L. Puma, C. Wang, P. Wang, W. Zhang and Q.Wang, *Appl. Catal. B–Environ.,* 2015, **168–169,** 25–32.
45 W. S. Choi, G. Y. Byun, T. S. Bae and H.–J. Lee, *ACS Appl. Mater. Interfaces,* 2013, **5,** 11225−11233.
46 Y. Tang, Z. Jiang, J. Deng, D. Gong, Y. Lai, H. T. Tay, I. T. K. Joo, T. H. Lau, Z. Dong and Z. Chen, *ACS Appl. Mater. Interfaces,* 2012, **4,** 438−446.
47 B. Li, H. Wang, B. Zhang, P. Hu, C. Chen and L. Guo, *ACS Appl. Mater. Interfaces,* 2013, **5,** 12283−12287.
48 Y. Bi and J. Ye, *Chem. Commun.,* 2009, 6551–6553.
49 H. Hu, Z. Jiao, G. Lu, J. Ye and Y. Bi, *RSC Adv.,* 2014, **4,** 31795–31798.
50 M. Zhu, P. Chen and M. Liu, *J. Mater. Chem.,* 2012, **22,** 21487–21494.
51 X. Liu, Z. Li, F. Li and Q. Qin, *Mater. Res. Bull.,* 2012, **47,** 1285–1288.
52 Q. Dong, Z. Jiao, H. Yu, J. Ye and Y. Bi, *CrystEngComm,* 2014, **16,** 8317–8321.
53 Y. Bi and J. Ye, *Chem. Eur. J.,* 2010, **16,** 10327–10331.
54 R. Dong, W. Liu and J. Hao, *Acc. Chem. Res.,* 2012, **45,** 504–513.
55 L. Qi, *Coord. Chem. Rev.,* 2010, **254,** 1054–1071.
56 J. Xiao and L. Qi, *Nanoscale,* 2011, **3,** 1383–1396.
57 R. Dong, B. Tian, C. Zeng, T. Li, T. Wang and J. Zhang, *J. Phys. Chem. C,* 2013, **117,** 213−220.
58 Y. Qiu, P. Chen and M. Liu, *J. Am. Chem. Soc.,* 2010, **132,** 9644–9652.
59 P. Guo, P. Chen and M. Liu, *Langmuir,* 2012, **28,** 15482−15490.
60 C. Zhang, P. Chen, H. Dong, Y. Zhen, M. Liu and W. Hu, *Adv. Mater.,* 2015, **27,** ASAP, DOI: 10.1002/adma.201501273.
61 Z. Tian, Q. Feng, N. Sumida, Y. Makita and K. Ooi, *Chem. Lett.,* 2004, **33,** 952−953.
62 T.–K. Huang, T.–H. Cheng, M.–Y. Yen, W.–H. Hsiao, L.–S. Wang, F.–R. Chen, J.–J. Kai, C.–Y. Lee and H.–T. Chiu, *Langmuir,* 2007, **23,** 5722−5726.
63 S. Han, W. Hou, W. Dang, J. Xu, J. Hu and D. Li, *Mater. Lett.,* 2003, **57,** 4520–4524.
64 S. Han, W. Hou, W. Dang, J. Xu, J. Hu and D. Li, *Colloid Polym. Sci.,* 2004, **282,** 761–765.
65 S.–H. Wu, C.–Y. Mou and H.–P. Lin, *Chem. Soc. Rev.,* 2013, **42**, 3862–3875.
66 H. Yoo and M. H. Jang, *Nanoscale,* 2013, **5,** 6708–6712.
67 Y. Guillemin, J. Ghanbaja, E. Aubert, M. Etienne and A. Walcarius, *Chem. Mater.,* 2014, **26,** 1848−1858.
68 J. Liu, A. Y. Kim, L. Q. Wang, B. J. Palmer, Y. L. Chen, P. Bruinsma, B. C. Bunker, G. J. Exarhos, G. L. Graff, P. C. Rieke, G. E. Fryxell, J. W. Virden, B. J. Tarasevich and L. A. Chick, *Adv. Colloid Interface Sci.,* 1996, **69,** 131–180.
69 P. K. Vinson, J. R. Bellare, H. T. Davis, W. G. Miller and L. E. Scriven, *J. Colloid Interface Sci.,* 1991, **142,** 74–91.
70 N. D. Petkovich and A. Stein, *Chem. Soc. Rev.,* 2013, **42**, 3721−3739.
71 L.–Z. Wu, B. Chen, Z.–J. Li and C.–H. Tung, *Acc. Chem. Res.,* 2014, **47,** 2177−2185.
72 Z.–Y. Zhou, N. Tian, J.–T. Li, I. Broadwell and S.–G. Sun, *Chem. Soc. Rev.,* 2011, **40,** 4167–4185.
73 K. Zhou and Y. Li, *Angew. Chem. Int. Ed.,* 2012, **51,** 602–613.
74 F. Zaera, *ChemSusChem,* 2013, **6,** 1797–1820.
75 M. Zhu, P. Chen and M. Liu, *J. Mater. Chem.,* 2011, **21,** 16413–16419.
76 X. Lu, C. Wang and Y. Wei, *Small,* 2009, **5,** 2349–2370.
77 W. Zhou, H. Liu, R. I. Boughton, G. Du, J. Lin, J. Wang and D. Liu, *J. Mater. Chem.,* 2010, **20,** 5993–6008.
78 M. Subhramannia and V. K. Pillai, *J. Mater. Chem.,* 2008, **18,** 5858–5870.
79 P. Roy, S. Berger and P. Schmuki, *Angew. Chem. Int. Ed.,* 2011, **50,** 2904–2939.
80 A. Kolmakov and M. Moskovits, *Annu. Rev. Mater. Res.,* 2004, **34,** 151–180.
81 Y. Wu, J. Yu, H.–M. Liu and B.–Q. Xu, *J. Nanosci. Nanotechnol.,* 2010, 10, 6707–6719.
82 M. Adachi, M. Sakamoto, J. Jiu, Y. Ogata and S. Isoda, *J. Phys. Chem. B,* 2006, **110,** 13872–13880.
83 H. Zhang, X. Lv, Y. Li, Y. Wang and J. Li, *ACS Nano,* 2010, **4,** 380–386.